

Antiviral drug acyclovir exhibits antitumor activity via targeting β TrCP1: Molecular docking and dynamics simulation study

Shagufta Shafique, Sajid Rashid*

National Centre for Bioinformatics, Quaid-i-Azam University, Islamabad, 45320, Pakistan



ARTICLE INFO

Article history:

Received 17 September 2016

Received in revised form

15 December 2016

Accepted 29 December 2016

Available online 31 December 2016

Keywords:

β TrCP1

ACV

Molecular docking

Molecular dynamics simulation

ABSTRACT

The critical role of β TrCP1 in cancer development makes it a discerning target for the development of small drug like molecules. Currently, no inhibitor exists that is able to target its substrate binding site. Through molecular docking and dynamics simulation assays, we explored the comparative binding pattern of β TrCP1-WD40 domain with ACV and its phospho-derivatives (ACVMP, ACVDP and ACVTP). Consequently, through principal component analysis, β TrCP1-ACVTP was found to be more stable complex by obscuring a reduced conformational space than other systems. Thus based on the residual contribution and hydrogen bonding pattern, ACVTP was considered as a noteworthy inhibitor which demarcated binding in the cleft formed by β TrCP1-WD40 specific β -propeller. The outcomes of this study may provide a platform for rational design of specific and potent inhibitor against β TrCP1, with special emphasis on anticancer activity.

© 2016 Elsevier Inc. All rights reserved.

1. Introduction

Nucleoside analogues (acyclovir, penciclovir, valacyclovir and famciclovir) are widely used as antiviral agents during active viral replication at host level. 9-(2-hydroxy-ethoxy-methyl) guanine (Acyclovir [ACV]) is a synthetic acyclic guanosine analog which is phosphorylated in the presence of virus and only accumulates in the infected cells. The normal host cells then convert it into diphosphate and triphosphate forms which inhibit viral DNA polymerase by competing with guanosine triphosphate and cause viral DNA chain termination [1]. ACV is pharmacologically active against Herpes simplex virus (HSV) types 1 and 2, Varicella Zoster virus (VZV) and Epstein Barr virus (EBV) which is moderately susceptible as EBV has minimal thymidine kinase activity [2]. Besides antiviral activity, recent study has proposed the potent antitumor activity of ACV-monophosphate (ACVP) derivative [3]. Encapsulation of ACVP by Lipid/Calcium/Phosphate (LCP) nanoparticles (NPs) facilitates its targeted delivery to the tumor cells for the inhibition of cell cycle progression and proliferation. The possible generality of this behavior has led to the suggestion that ACV and its phospho-derivatives may be of potential therapeutic value against oncotargets.

In this study, the structural basis of β TrCP1 inhibition has been elucidated through binding of ACV and its phospho-derivatives. The

F-box protein, β TrCP1 is one of the four subunits of SCF (Skp1-Cullin-1-F-Box) ubiquitin E3 ligase complex that shifts ubiquitin molecules to tag substrates for proteasome degradation. Recently, elevated levels of β TrCP1 have been observed in various cancers including prostate, breast, pancreatic, melanoma and colorectal cancer [4–7]. The oncogenic role of β TrCP1 has been well addressed through targeted degradation of various growth and survival factors [8]. Moreover, recent study attributed a central role of β TrCP1 in triggering degradation events of multiple proteins (DCHS1, ARID1A, PCDHB1, PCDHB12 and IL12RB1) via ubiquitin-mediated pathway [9]. Thus inhibition of β TrCP1 substrate binding ability may be a promising strategy for cancer therapy.

In view of these observations, there is a dire need to develop potent small molecular inhibitors to target β TrCP1. Previously, multiple inhibitors have been reported which are involved in preventing β TrCP1-mediated substrate ubiquitination [10,11]. These inhibitors are reliant upon their means of action to disrupt SKP1- β TrCP1 interaction and hinder the activity of CRL1 β TrCP1 by interfering with substrate degradation [12]. However, to date, no specific inhibitor has been reported which is exclusively able to target β TrCP1-WD40 domain. β TrCP1 exhibits two vital target sites, an N-terminal F-box domain and a C-terminal WD40 repeat containing domain [13,14], that is critical for its binding to diverse substrates. A thorough understanding of structural details and functional activity of β TrCP1 could be a benchmark for the identification of specific and more potent β TrCP1 inhibitors. To accomplish these tasks, we applied integrative virtual screening approach

* Corresponding author.

E-mail address: sajidrwp@yahoo.co.uk (S. Rashid).

through combined pivotal structural insight of β TrCP1-WD40 specific substrate binding site via molecular dynamics simulation assays.

2. Methodology

2.1. Data set

Crystal structure of human β TrCP1 (PDB entry: 1P22) was retrieved through PDB (Protein data bank) database [15]. 2D structures (SDF format) of ACV (PubChem ID: 2022), ACVMP (Acyclovir monophosphate; PubChem ID: 83999), ACVDP (Acyclovir diphosphate; PubChem ID: 501523) and ACVTP (Acyclovir triphosphate; PubChem ID: 84000) were retrieved through PubChem database [16] and converted into PDB format through PyMol (<http://www.pymol.org>) (Fig. 1). The scrutinized compounds were then subjected to geometry optimization through Avogadro tool [17] to assign proper protonation and stereoisomerization.

2.2. Molecular docking analysis

The selected compounds (A–D) were virtually docked against β TrCP1-WD40 domain through AutoDock 4.2 [18] suit of PyRx to achieve an optimal complementarity of steric and physiochemical properties. The number of runs for each docking procedure was set to 150. The Lamarckian genetic algorithm (LGA) was applied with the following parameters: initial population of 150 randomly placed individuals, a maximum number of 27,000 generations, a mutation rate of 0.02, 2.5×10^6 energy evaluations and a crossover rate of 0.80, while the remaining docking parameters were set to default. To attain the best compounds through comparative docking approach, these compounds were further validated through GOLD (Genetic Optimization for Ligand Docking) [19]. GOLD uses stochastic manner to explore ligand positions and conformations. It implements genetic algorithm to build the ideal model during docking procedure [20,21]. The compounds were docked against β TrCP1 using the Goldscore function and redocked using the Chemscore function, as described elsewhere [22]. The generated log files were used to sort out the ranked compounds on the basis of Goldscore and Chemscore scoring functions [23]. LigPlus [24] and UCSF Chimera ver. 1.10.0 [25] tools were used to visualize the receptor-ligand hydrogen bonding and hydrophobic interactions.

2.3. Molecular dynamics simulation analysis

Next, molecular dynamics (MD) simulations were performed using the apo and inhibitor bound states of β TrCP1-WD40 domain (β TrCP1-ACV, β TrCP1-ACVMP and β TrCP1-ACVTP) to explore the dynamic nature of interactions and to dissect the comparative structural constraint between apo- β TrCP1 and inhibitor bound states. Groningen Machine for Chemicals Simulations (GROMACS) 5.0.7 package was used to perform MD simulation assays [26]. PRODRG tool [27] was utilized for topology file generation and force field parameterization of drug molecules. All MD simulations were performed using GROMOS96 43A1 force field [28] to acquire the equilibrated system. Systems were solvated using SPC water model [29] in a periodic box using a minimum distance of 1.4 nm, followed by energy minimization (steepest descent algorithm for 500 steps), via a tolerance of 1000 kJ/mol Å² to remove initial steric clashes. The energy minimized systems were treated for 1000 ps equilibration run under pressure and temperature conditions to relax the systems. Finally, MD simulations were run for 20 ns time scale under constant temperature (300 K) and pressure (1 atm). PME (Particle Mesh Ewald) algorithm was used in all calculations to dissect electrostatic interactions [30]. Stability and time dependent behavior of each system was investigated at various time scales. GROMACS

modules such as g_rms, g_rmsf, g_energy and g_hbond functions were utilized to analyze the stability and behavior of each system. All MD trajectories were analyzed using UCSF Chimera ver. 1.10.0 and PyMol. DSSP tool was utilized to assign the secondary structure for each tiem frame [31].

2.4. Principal component analysis

Principal component analysis (PCA) was performed through g_covar and g_anaeig modules of GROMACS to interpret the principal modes convoluted in the motion of proteins [32]. The covariance matrix was congregated via simple linear alteration in Cartesian coordinate space. A vectorial representation of each particular constituent of the motion specifies the trend of motion. Consequently, a set of eigenvectors was acquired through the diagonalization of the covariance matrix. For each eigenvector, a particular eigenvalue defined the energetic influence of component to the motion [33]. The protein regions that were accountable for the utmost notable cooperative motions were predicted through PCA.

3. Results

3.1. Binding characterization of ACV inhibitors into binding pocket of β TrCP1

The objective of the current study is based on the exploration of novel inhibitors for β TrCP1 via bioinformatics analysis. Molecular docking approach, one of the trustworthy approaches in drug discovery process was used to explore the binding of β TrCP1 with ACV and its derivatives at the substrate binding cleft. Initially, docking analysis was accomplished with 150 runs and the ideal conformer having lowest binding energy value was selected for further analysis (Table 1). Overall, docking analysis of ACV and its phospho-derivatives revealed more affinity for ACVTP at the β TrCP1 substrate binding site, followed by ACVMP (Fig. 2).

In β TrCP1-ACV complex (GOLD score: 57.47), hydrogen bond formation occurred between Leu311 of β TrCP1 and ACV specific N⁴-atom of guanine ring. Moreover, Arg524 formed hydrogen bonds with O²-atom of ethoxy group and N⁵-atom of guanosine moiety (Fig. 2A). Tyr271, Cys272, Leu351, His352, Val395, Ala434 Cys435, Leu436, Arg474, Cys475 and Ile476 residues of β TrCP1 were involved in hydrophobic association with ACV.

Docking analysis revealed placement of ACVMP in the binding cavity of β TrCP1 by orienting guanosine ring deep into the central channel, while the ethyl phosphate moiety was pointed to the upper face of the β -propeller (Fig. 2B). Tyr271, Leu311, Leu313, Leu351, His352, Asn394, Arg474 and Arg524 residues of β TrCP1 were observed in polar and hydrophobic contacts with ACVMP. The Arg474 residue of β TrCP1 was observed in hydrogen bonding with O⁶ and O³ atoms of ACVMP, while Leu313 residue was involved in hydrogen bonding with N⁵-atom of inhibitor.

The ideal docked conformer of ACVDP showed binding at the top face of the β -propeller with a binding score of -5.38 kcal/mol and GOLD score of 93.27 (Fig. 2C). The detailed binding analysis of this binding pose revealed the formation of hydrogen bond between guanine ring of ACVDP and Arg474 residue of β TrCP1. Similarly, two O-atoms (O⁸ and O⁴) of diphosphate moiety were implicated in hydrogen bonding with the guanidinium groups of Arg410 and Arg431 residues, respectively. Furthermore, Leu351, Asn394, Gly408, Ser448, Leu472 and Tyr488 residues were observed in van der Waals interactions.

A thorough analysis of the best β TrCP1-ACVTP conformer (GOLD score: 108.14) elucidated binding in a manner consistent with the binding of ACVMP and β TrCP1. The guanosine moiety of ACVTP obscured well within the binding cavity of β TrCP1. Concisely,

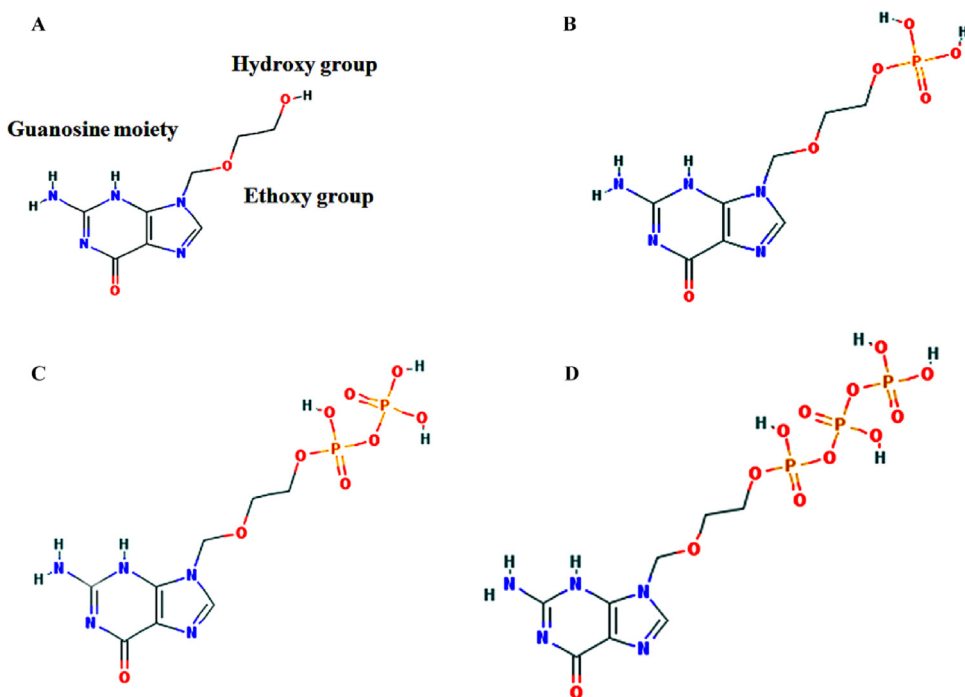


Fig. 1. 2D structures of compounds. (A) ACV, (B) ACVMP, (C) ACVDP and (D) ACVTP.

Table 1

Energy scoring values and binding residues of β TrCP1 with selected compounds.

Compounds	AutoDock score (kcal/mol)	GOLD score	Binding residues
ACV	-4.36	57.47	Tyr271, Cys272, Leu311 , Leu351, His352, Val395, Ala434 Cys435, Leu436, Arg474, Cys475, Ile476, Arg524
ACVMP	-4.71	72.35	Tyr271, Cys272, Leu311, Cys312, Leu313 , Leu351, His352, Leu353, Asn394, Val395, Ala434, Cys435, Arg474 , Cys475, Phe523, Arg524
ACVDP	-5.38	93.27	Leu351, Asn394, Gly408, Arg410 , Arg431 , Ser448, Leu472, Arg474 , Tyr488
ACVTP	-6.67	108.14	Tyr271, Cys272, Leu311, Cys312, Leu351, His352, Asn394, Ala434, Arg474 , Cys475, Tyr488 , Phe523, Arg524

we observed the presence of one hydrogen bond between O²⁻-atom of ACVTP and Arg521 specific guanidinium group. Similarly, O¹¹-atom formed a charged stabilized hydrogen bond with gate keeper residue, Arg474. Another hydrogen bond was observed between O¹¹-atom of the triphosphate moiety and hydroxyl group of Tyr488 residue. Additionally, β TrCP1-ACVTP complex exhibited a favorable number of hydrophobic interactions through Tyr271, Cys272, Leu311, Cys312, Leu351, His352, Asn394, Ala434, Cys475 and Phe523 residues.

Overall, structural insight of β TrCP1-WD40 domain revealed momentous role of hydrophobic regions and key polar residues of β -propeller in the cooperative binding. Furthermore, hydrogen bonds were also noticeable other than hydrophobic interactions thereby stabilizing the interaction.

3.2. Molecular dynamics simulation analysis

β TrCP1-ACV, β TrCP1-ACVMP and β TrCP1-ACVTP complexes were further characterized by dynamics simulation assays to investigate the stability, folding, conformational alterations and dynamic behavior of β TrCP1 upon inhibitor binding into the substrate binding cavity. Dynamic trajectories of each simulated system were thoroughly investigated to assess the stability and conformational changes by plotting the RMSD (Root Mean Square Deviations),

RMSF (Root Mean Square Fluctuations), Rg (Radius of gyration), RDF (Radial Distribution Functions), hydrogen bond, energy and secondary structure plots.

The overall stability of each complex was measured by estimating the RMSD profile which showed a quite stable interaction behavior. All systems observed over a time scale of 20 ns were quite stable throughout simulations (Fig. 3A–B). In case of β TrCP1-ACVTP complex, RMS deviations were much reduced as compared to other simulated complexes. The average RMSD values of system-derived C-alpha atoms were below 2.7 Å, suggesting the overall system stability. β TrCP1-ACVTP complex was further evaluated until 55 ns and similar trend of system was observed as before. Correspondingly, Rg profiles of individual systems were consistent with their resultant RMSD profiles (Fig. S1). A higher Rg value implies lower compactness of a system [34]. Consequently, β TrCP1-ACVTP exhibited minor compactness than apo-form. In contrast, ACVMP exhibited more compactness and stability. Accordingly, higher Rg values of bound complexes than that of apo- β TrCP1 suggested that firmness resulted in synergic conformational adaptation owing to β TrCP1 interaction with ACV, ACVMP and ACVTP.

RMSF values compute the extent of residual fluctuation, denoted by the peak elevation. RMSF plots indicated residual flexibility upon β TrCP1 binding to inhibitors (Fig. 3C). In case of β TrCP1-ACV, major fluctuations were observed in Asn295, Thr296 and

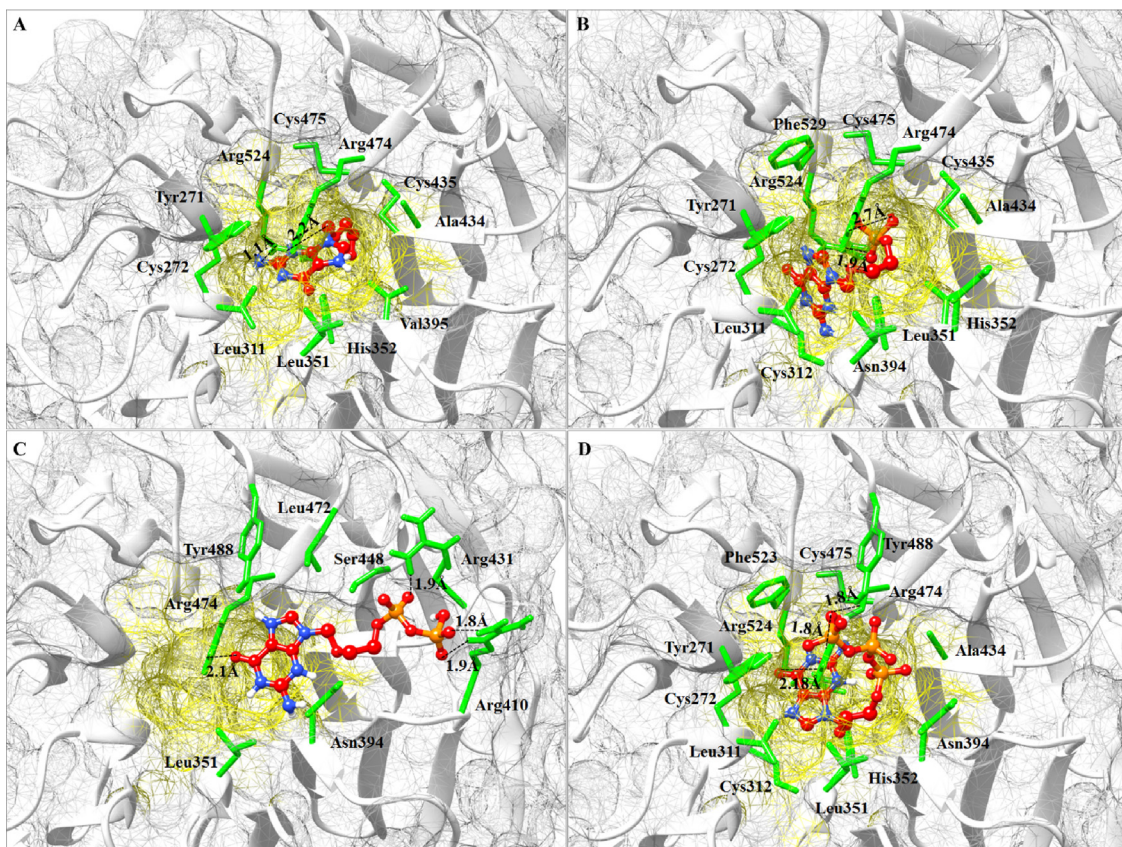


Fig. 2. Binding mode analyses. Best docked complexes of (A) β TrCP1-ACV, (B) β TrCP1-ACVMP, (C) β TrCP1-ACVDP and (D) β TrCP1-ACVTP. β TrCP1 is shown in gray ribbon, while interacting residues are represented in green sticks. The binding pocket is shown by yellow meshwork. Inhibitor atoms/bonds are shown in red ball and stick representation and hydrogen bonds are shown by dotted lines with calculated distance in angstrom. (For interpretation of the references to colour in this figure legend, the reader is referred to the web version of this article.)

Arg504-Ala507 residues within a range of 3 Å. In case of β TrCP1-ACVMP, loop region (Asp506-Gly508) showed major fluctuation up to 4.5 Å (Fig. 3D). The residues involved in ACV binding namely Tyr271, Cys272, Leu311, Cys312, Leu313, Leu351, His352, Leu353, Asn394, Val395, Ala434, Cys435, Arg474, Cys475, Phe523 and Arg524 displayed lower fluctuations, indicating more stability with a pronounced role in interaction (Fig. 3C).

Correspondingly, in β TrCP1-ACVTP, significant fluctuations were detected in Ser267, Glu517 and Ser519 residues, located in immediate vicinity of binding residues (Fig. 3D). However, critical residues (Tyr271, Cys272, Leu311, Cys312, Leu351, His352, Asn394, Ala434, Arg474, Cys475, Tyr488, Phe523 and Arg524) involved in ACVTP binding were quite stable. RMSF results indicated that pronounced residual fluctuations were present in loop regions, while relatively minor fluctuations were observed in the β -sheets or α -helical regions of β TrCP1.

MD simulation trajectory files of β TrCP1 and inhibitor complexes were subjected to energy calculation. LJ-SR energy has been deliberated as a trustworthy binding descriptor [9]. As described in energy plot, all systems were well equilibrated and remained stable throughout MD simulations (Fig. 4A). The β TrCP1-ACVTP complex exhibited more energy value (-1400 kcal/mol), compared to other complexes. Generally, LJ-SR energy (-1600 to -900 kcal/mol) values were relatively stable (Fig. 4A).

The binding characteristics of β TrCP1 with ACV, ACVMP and ACVTP were examined through plotting time-dependent intermolecular hydrogen bonds. In contrast to β TrCP1-ACV and β TrCP1-ACVMP systems, more intermolecular hydrogen bonds were observed in β TrCP1-ACVTP, specifying higher interaction (Fig. 4B). Inclusively, hydrogen bond interaction pattern remained

stable during the entire simulation time. These data validated that ACVTP exhibited more stable binding with β TrCP1 as compared to ACV and ACVMP.

RDF profile was calculated for β TrCP1 specific Arg474 and Arg524 residues in comparison to Ala434 residue which was located at the base of pocket (Fig. 4C-D). RDF provided relative affinities among atomic sets in the system. The radial function $G(r)$ was calculated, where (r) is the distance of Arg474 and Arg524 residues with respect to average position of Ala434 residue.

3.3. Secondary structure profile analysis

The secondary structure profile analysis of the three complexes (β TrCP1-ACV, β TrCP1-ACVMP and β TrCP1-ACVTP) and apo- β TrCP1 was carried out using the DSSP tool (Fig. 5). Evidently, in ACVTP, the turn region encompassing Trp455-Val465 residues of β TrCP1 was transformed into bend and coil as compared to apo-form (Fig. 5). In β TrCP1-ACV and β TrCP1-ACVMP complexes, this region remained structurally preserved (Fig. 5B-C). Another notable secondary structural amendment was witnessed in the loop region of β TrCP1, where Ala500-Leu512 residues adopted an α -helical conformation upon binding to ACV derivatives. Similarly, Ala507-Leu510 region was converted into α -helix (Fig. 5E). β -sheet conformations remained stable throughout the simulation period.

A considerable conformational change in β TrCP1 was observed at the region encompassing Val350-Asn356 residues, resulting in the shortening of β 9-strand. Other profound conformational changes were observed in β 21 and β 25 strands of β TrCP1 (Fig. S2), as upon ACVTP binding, these β -strands were completely missing. Likewise, in β TrCP1-ACVMP complex, significant conformational

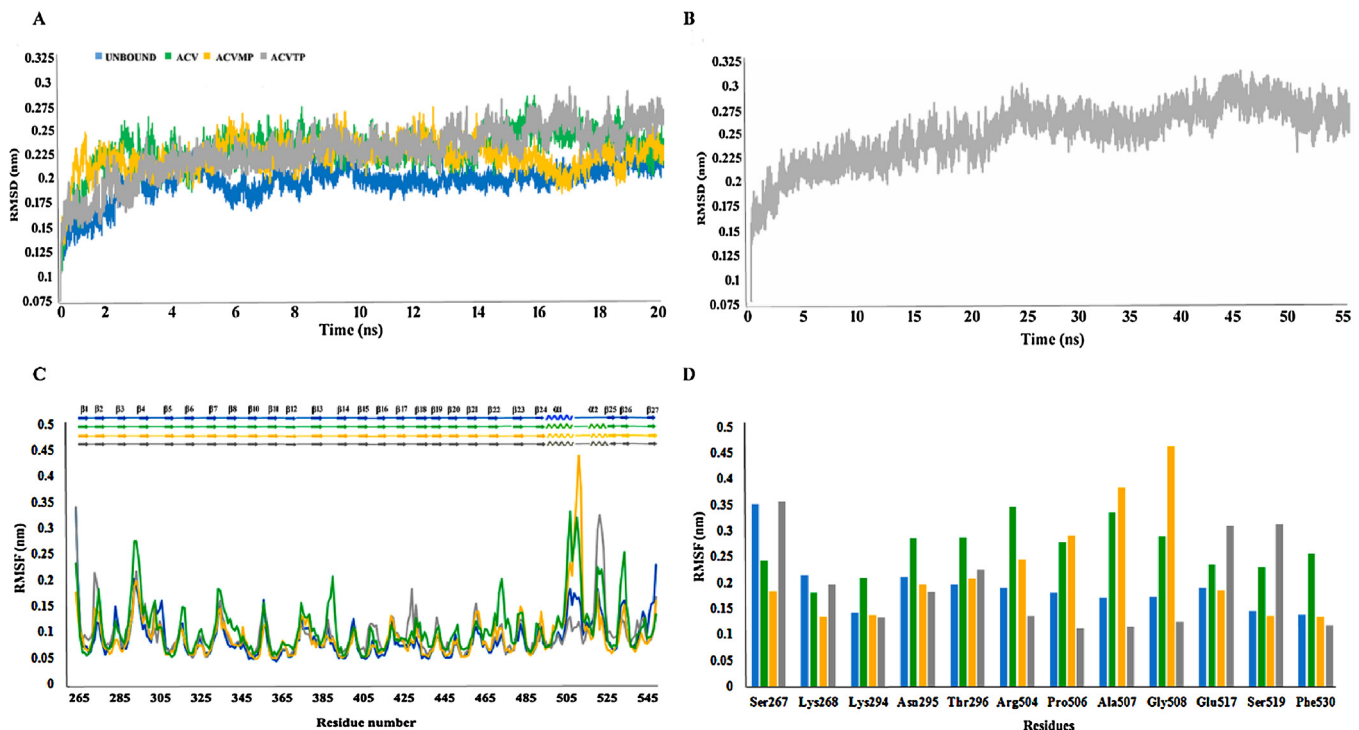


Fig. 3. RMSD and RMSF plots for 20 ns MD simulations to investigate stability and fluctuation of bound and apo- states of β TrCP1. RMSD plots were computed through least square fitting of backbone $C\alpha$ -atoms. (A) Apo- β TrCP1 and bound forms (β TrCP1-ACV, β TrCP1-ACVMP, β TrCP1-ACVDP and β TrCP1-ACVTP) are illustrated in blue, green, goldenrod and gray colors, respectively. (B) RMSD plot over a time scale of 55 ns. (C) Comparative RMSF plots of apo- β TrCP1 (blue), β TrCP1-ACV (green), β TrCP1-ACVMP (goldenrod) and β TrCP1-ACVTP (gray). Secondary structures are illustrated above the plots in corresponding colors. Arrows demarcate β -strand and coils delineate α -helices. (D) Comparison of fluctuating residues for all systems is indicated by bar chart. (For interpretation of the references to colour in this figure legend, the reader is referred to the web version of this article.)

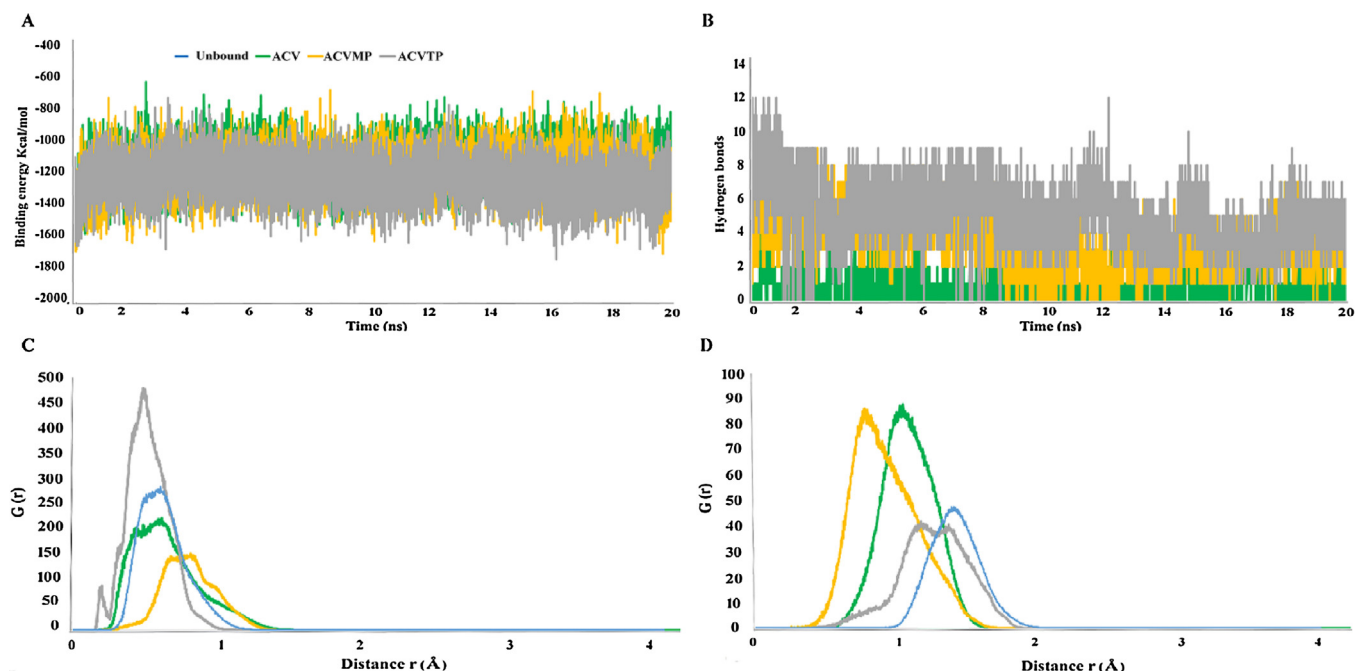


Fig. 4. Time-dependent analysis of MD trajectories and radial distribution function curves for β TrCP1 gate keeper residues. (A) Energy plots for β TrCP1-ACV, β TrCP1-ACVMP and β TrCP1-ACVTP complexes are shown in green, goldenrod and gray color, respectively. (B) Intermolecular hydrogen bonds formed between binding residues of β TrCP1 in complex with ACV, ACVMP and ACVTP. Radial distribution function $G(r)$ for (C) Arg474 and (D) Arg524 residues of β TrCP1 to α -carbon atom of Ala434 for the three simulated systems, ACV (green), ACVMP (goldenrod) and ACVTP (gray). “r” is the distance of key residues from the average position of Ala434 residue. (For interpretation of the references to colour in this figure legend, the reader is referred to the web version of this article.)

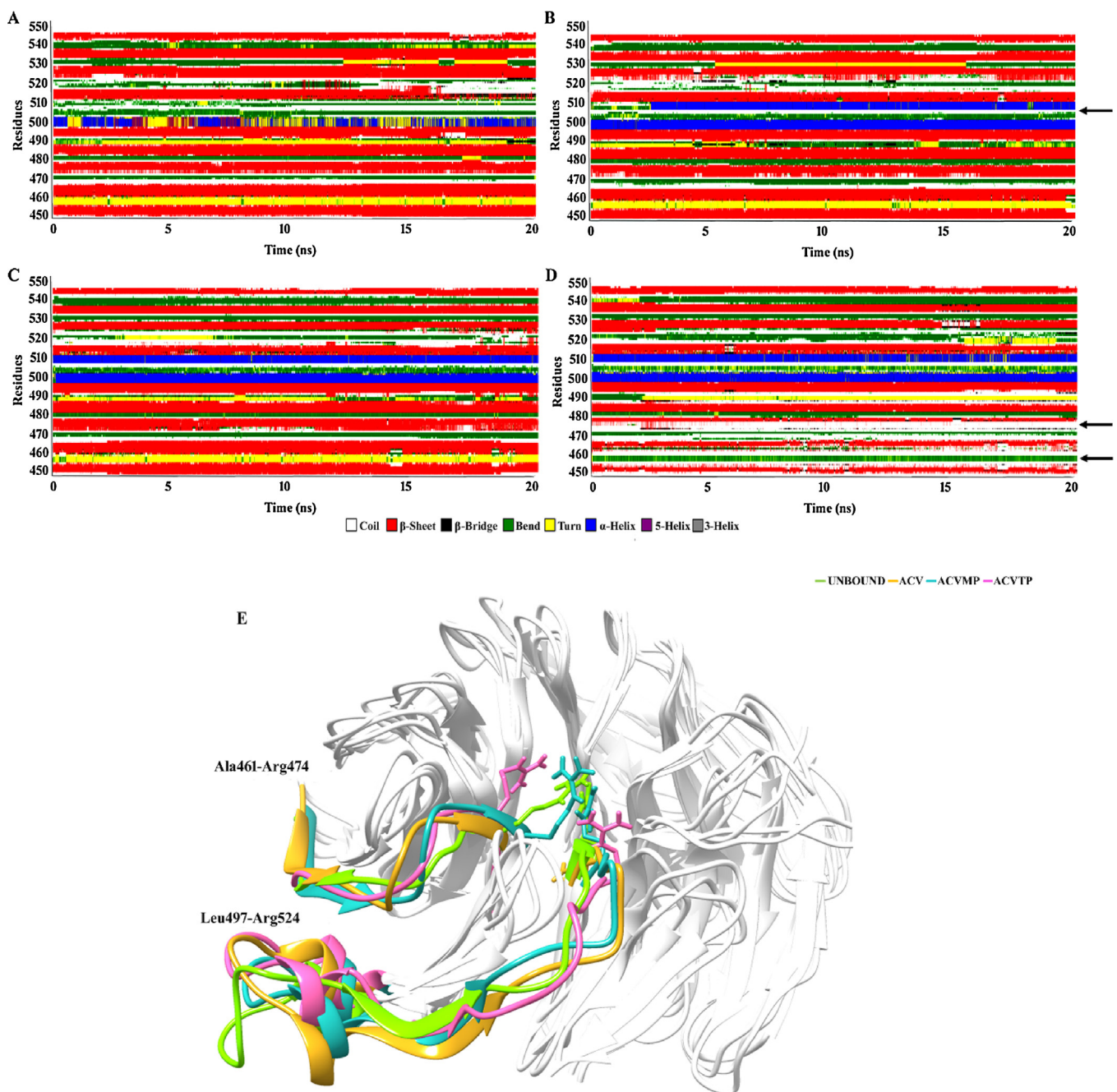


Fig. 5. DSSP specific secondary structure assignment for 20 ns total simulation time. (A) apo- β TrCP1, (B) β TrCP1-ACV, (C) β TrCP1-ACVMP, (D) β TrCP1-ACVTP and (E) Superimposition of apo- and inhibitor bound complexes of β TrCP1 (white ribbon). The regions encompassing conformational readjustments are marked with green, golden rod, sea green and pink colors for β TrCP1, β TrCP1-ACV, β TrCP1-ACVMP and β TrCP1-ACVTP complexes, respectively. Binding residues are indicated by stick representation. (For interpretation of the references to colour in this figure legend, the reader is referred to the web version of this article.)

readjustments were observed in Phe422-Tyr425, Ile433 and Ala434 residues, which resulted in the conversion of β -strands into loops to accommodate the inhibitor. Similarly, Ala507-Leu510 residues of β TrCP1 lying in the loop region were transformed into α -helical conformation due to inhibitor binding. Other than these variations, α -helices remained intact and stable during the entire simulation period.

To characterize the pronounced conformational switches in comparison to apo- β TrCP1 and β TrCP1-ACVTP complex, PDB files were generated at 1, 5, 10, 15 and 20 ns time scales. Substantial conformational alterations were witnessed in the vicinity of binding pocket (Fig. 6). Particularly, widening of β TrCP1 specific binding cavity was evident to accommodate ACVTP, where guano-

sine group settled well into the hollow cavity, while triphospho group was moved adjacent to the cavity opening (Fig. 6D). Upon ACVTP binding, Arg524 residue of β TrCP1 was significantly pushed outward which opened the binding pocket and conformational space acquired by the inhibitor. This structural twist bowed down Arg524 residue towards the inhibitor and improved the interaction via hydrogen bonding. Similarly, gatekeeper residue, Arg474 was significantly twisted outward (Fig. 6D), thus creating a doorway for the appropriate entrance of inhibitor inside the cavity and aiding in the formation of a conventional hydrogen bond with triphosphate group. These structural arrangements altered the placement of Tyr271 residue which bent towards the inhibitor to increase the binding affinity. Likewise, placement of guanosine moiety in the

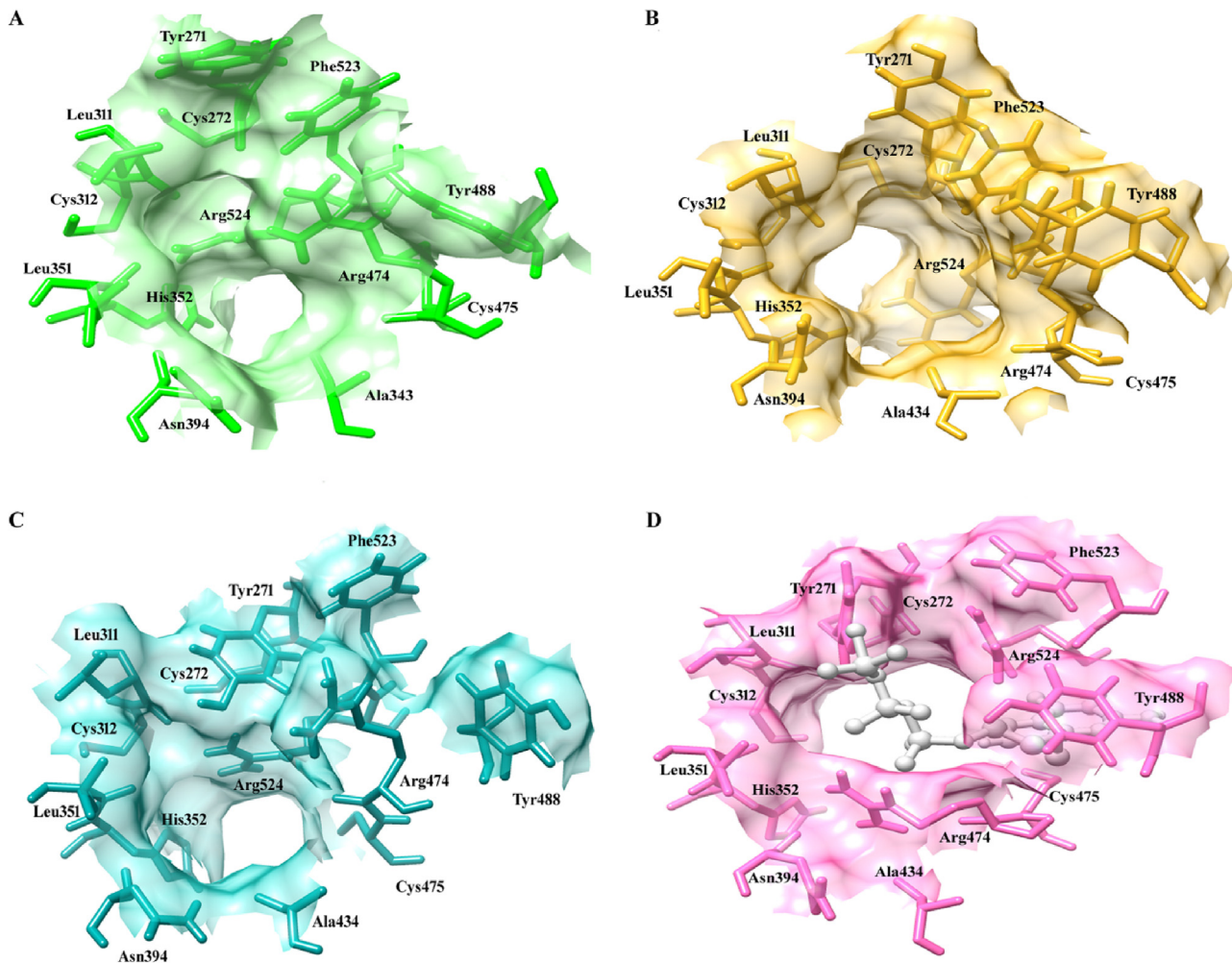


Fig. 6. Conformational changes in β TrCP1-WD40 domain upon ACVTP binding. Binding pocket insight of (A) apo- β TrCP1 (light green), (B) β TrCP1-ACV (goldenrod), (C) β TrCP1-ACVMP (sea green) and (D) β TrCP1-ACVTP complex (pink) is depicted in surface views, respectively. The binding cavity residues are indicated in stick representation and labelled accordingly, while bound inhibitor is shown in gray ball and stick representation. (For interpretation of the references to colour in this figure legend, the reader is referred to the web version of this article.)

close proximity of Tyr488 resulted in the tilted movement of loop which fetched Tyr488 closer to the inhibitor thus making a stacking interaction. The re-positioning of Arg474 and Arg524 residues was further elaborated by the time-dependent distance plots of gatekeeper residues (Fig. 7A).

Overall, interaction pattern of β TrCP1-ACVTP complex suggested that ACVTP binding recruited the positional facilitation of Arg474, Tyr488 and Arg521 residues in the binding cavity thus sustaining the binding stability of β TrCP1. However, this trend was not visible in other systems (Fig. 7B). The mutual binding of ACVTP and substrates at similar residues of β TrCP1 suggested that ACVTP may compete for the substrate binding site of β TrCP1 to influence its activity.

3.4. Principal component analysis

Principal component analysis (PCA) was performed using apo and inhibitor bound β TrCP1 to monitor the overall strenuous motions, required for the activity of protein. A covariance matrix of 843 backbone $C\alpha$ -atoms was generated for each simulated system (apo- β TrCP1, ACV- β TrCP1, ACVMP- β TrCP1 and ACVTP- β TrCP1) to capture the degree of inhibitor co-linearity in the atomic positions for 281 residues within β TrCP1 structure for each pair of atoms. Eigenvectors and eigenvalues were acquired through the diag-

nizable covariance matrix of backbone $C\alpha$ -atoms. Eigenvectors describe a cooperative motion attained by the particles. The eigenvectors with the top two eigenvalues were considered as the first and second principal components, respectively.

The overall flexibility was calculated by the trace of diagonalized covariance matrix. The projection of first two principal components demonstrated the motion of apo- β TrCP1, β TrCP1-ACV, β TrCP1-ACVMP and β TrCP1-ACVTP complexes in phase space with the trace values of 10.2 nm^2 , 13.0 nm^2 , 11.2 nm^2 and 10.6 nm^2 , respectively. The direction of motion was denoted by the eigenvectors and the aggregate motion beside eigenvectors was signified by eigenvalues. Dissemination of more dots in the plot manifested the conformational alterations of β TrCP1 in apo as well as in the bound form of β TrCP1. β TrCP1-ACV complex displayed a higher trace value signifying an overall intensification in the flexibility than the apo- β TrCP1, whereas β TrCP1-ACVTP divulged the lowest values endorsing a flexibility decline in the shared motion of β TrCP1. Consequently, from these projections, it was perceived that β TrCP1-ACVTP clusters were well demarcated and more stable compared to other systems. The β TrCP1-ACVTP obscured a smaller region of conformational space than the apo-form or other simulated systems (Fig. 8).

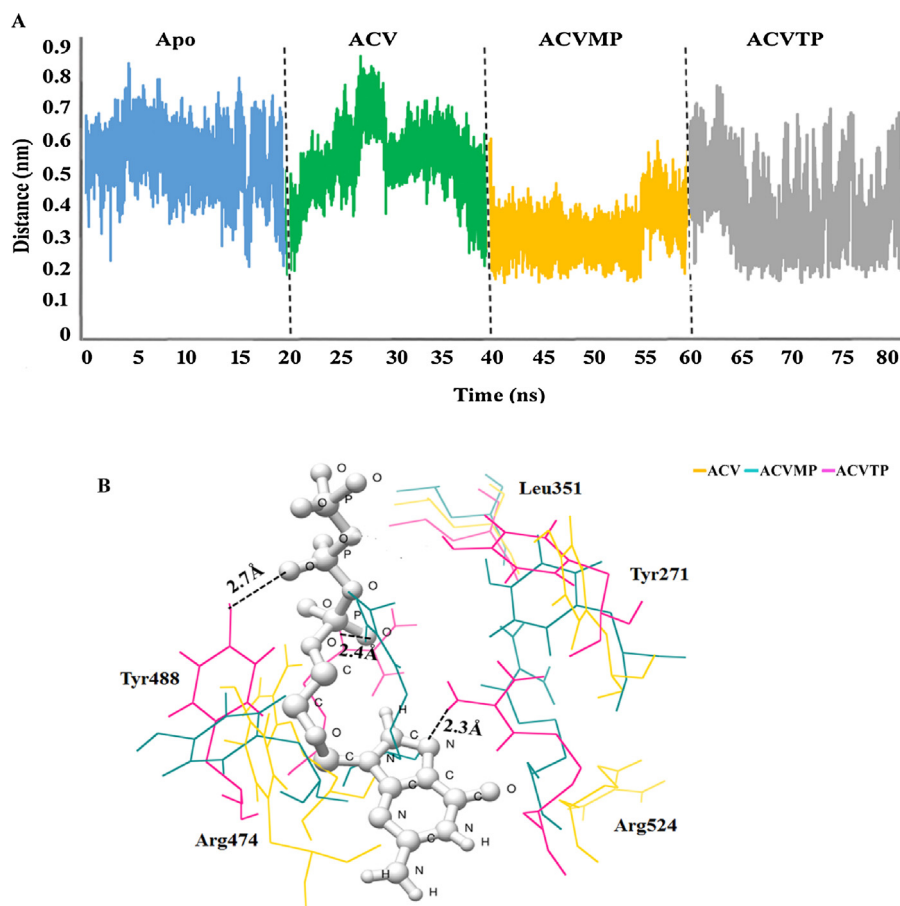


Fig. 7. Time-dependent distance plots between Arg474 and Arg524 residues. (A) Distance plots between Arg474 and Arg524 residues for apo- β TrCP1 (blue), β TrCP1-ACV (green), β TrCP1-ACVMP (gold) and β TrCP1-ACVTP (gray) over 20 ns time period. (B) Structural adaption of β TrCP1 binding residues upon interaction with ACVTP. Snapshot was taken at 15 ns time interval of MD simulation. Labeled residues of apo- β TrCP1 (green), β TrCP1-ACV (gold), β TrCP1-ACVMP (sea green) and β TrCP1-ACVTP (pink) are represented in wire form. ACVTP is indicated in gray color. Hydrogen bonds of β TrCP1-ACVTP are represented by black dotted lines with bond distances in angstrom. (For interpretation of the references to colour in this figure legend, the reader is referred to the web version of this article.)

4. Discussion

WD40 domain containing proteins serve as transient interplay platforms to bridge protein-DNA interactions [35] via their seven-bladed β -propeller. These proteins act as key regulators of several biological processes such as gene expression, signal transduction, ubiquitination, histone modification, genome stability, apoptosis and cell cycle control [36]. The β -propeller binds to the substrate recognition motifs of phosphorylated proteins known as phosphodegrons [9]. The unique role of WD40 proteins in the substrate selectivity and its targeting to E3-ubiquitin ligases [37] makes them attractive candidates for targeted therapy. Particularly, CRLs [Cullin-RING (really interesting new gene) E3-ubiquitin ligases] are of particular interest being the largest family of E3-ligases [38]. Despite growing structural and functional knowledge of these multicomponent ligases, their specifically targeting small-molecule inhibitors are still lacking. In this study, we characterized binding of ACV and its phospho-derivatives with β TrCP1 ubiquitin ligase, via thorough understanding of its structural assembly and configuration. Subsequently, a detailed interaction analysis of selected inhibitors by structure-guided approaches demarcated their presence in the binding cleft formed by inter-bladed binding grooves of β -propeller.

Strikingly, Arg524 and Arg474 residues of β TrCP1 were actively engaged in interactions with ACV and its phospho-derivatives via hydrogen bonding (Table 1). Moreover, a consistent behavior of Tyr271, Cys272, Leu311, Leu351, His352, Ala434, Arg474, Cys475

and Arg524 residues was witnessed throughout dynamics simulations which emphasized the adequate β TrCP1 selectivity via cooperative binding with inhibitors. The compelling evidence of β TrCP1 specific residual (Arg474, Tyr488 and Arg524) involvement in both inhibitor and substrate binding equates the recognition of doubly phosphorylated destruction motif [9,39] with inhibitor binding paradigm. It stands to reason that the selected inhibitors may intensely compete for the substrate binding cavity of β TrCP1.

A thorough comparison of apo- β TrCP1 and β TrCP1-ACVTP complex uncovered the dynamic behavior and structural constraints of substrate binding pocket which emphasized substantial conformational changes in Tyr271, Arg474, Tyr488 and Arg524 residues of β TrCP1. These residues were involved in hydrogen bonding with ACVTP and rendered its specific entrance into the binding cavity. The prominent conformational readjustments of β -strands localized in 5–7 blades of β -propeller imparted mechanistic role in the opening of binding cavity to accommodate the inhibitor. These changes were not observed in case of β TrCP1-ACV and β TrCP1-ACVMP complexes.

Collectively, findings in this work would provide novel insight into the structural and mechanistic basis of β TrCP1 targeting supported by MD simulation studies. In view of deep structural analysis, we propose that ACVTP may prove to be more effectual inhibitor for β TrCP1 targeted therapy, consequently abolishing β TrCP1 ligase activity toward ubiquitination of substrates.

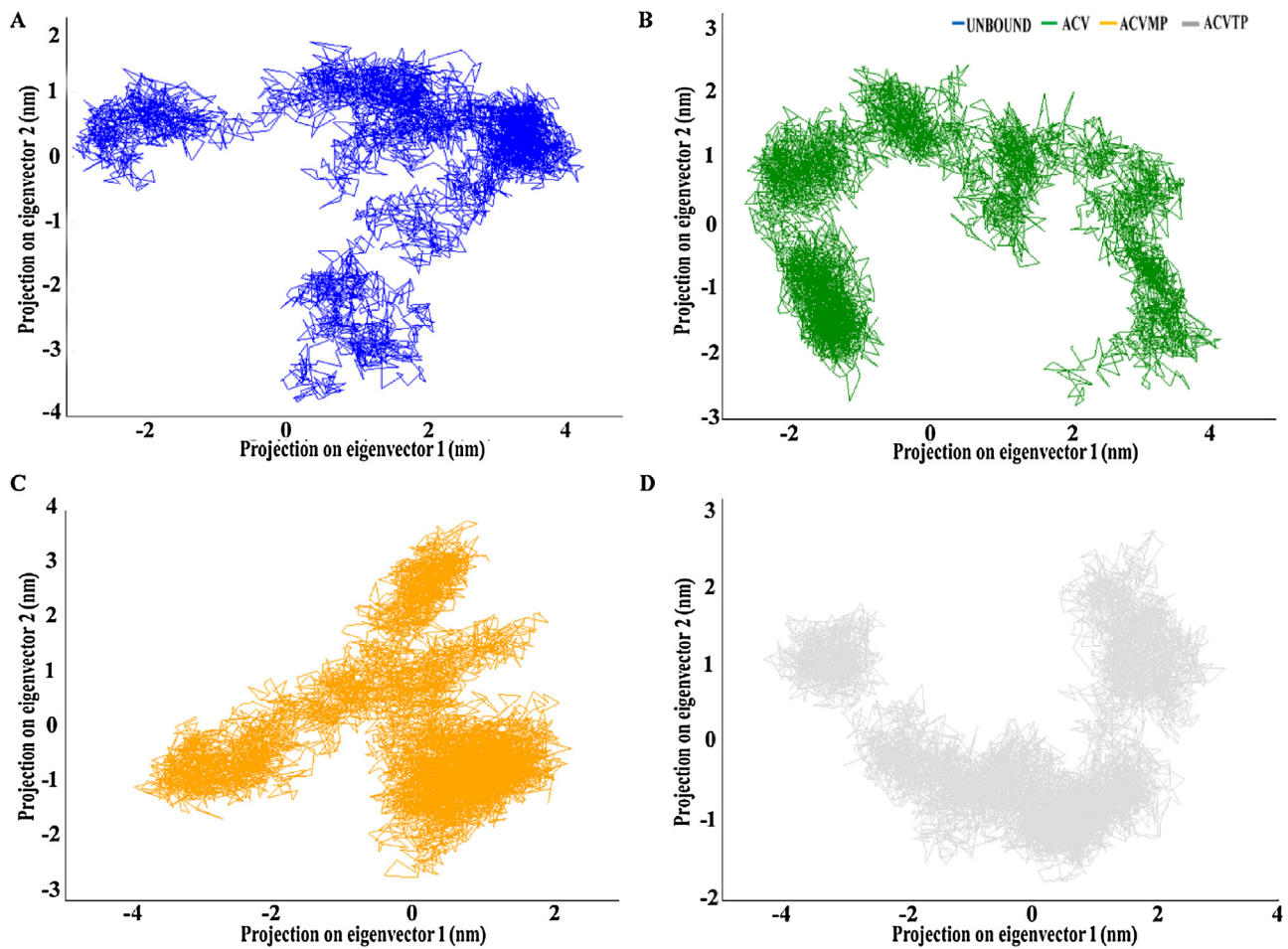


Fig. 8. 2D projection of the motion of apo and inhibitor bound β TrCP1 over the first two principal components. (A) Apo- β TrCP1, (B) β TrCP1-ACV, (C) β TrCP1-ACVMP and (D) ACVTP.

Conflict of interest

The authors declare that they have no competing interests.

Acknowledgements

We thank Saima Younis, Hafsa Niaz and Rafia Raja for critical reading of the manuscript.

Appendix A. Supplementary data

Supplementary data associated with this article can be found, in the online version, at <http://dx.doi.org/10.1016/j.jmgm.2016.12.018>.

References

- [1] G.B. Elion, Mechanism of action and selectivity of acyclovir, *Am. J. Med.* 73 (1982) 7–13.
- [2] N. Coen, S. Duraffour, K. Haraguchi, J. Balzarini, J.J. van den Oord, R. Snoeck, G. Andrei, Antiherpesvirus activities of two novel 4'-thiothymidine derivatives, KAY-2-41 and KAH-39-149, are dependent on viral and cellular thymidine kinases, *Antimicrob. Agents Chemother.* 58 (2014) 4328–4340.
- [3] J. Yao, Y. Zhang, S. Ramishetti, Y. Wang, L. Huang, Turning an antiviral into an anticancer drug: nanoparticle delivery of acyclovir monophosphate, *J. Control Release* 170 (2013) 414–420.
- [4] A. Koch, A. Waha, W. Hartmann, A. Hrychyk, U. Schüller, A. Waha, K.A. Wharton Jr., S.Y. Fuchs, D. von Schweinitz, T. Pietsch, Elevated expression of Wnt antagonists is a common event in hepatoblastomas, *Clin. Cancer Res.* 11 (2005) 4295–4304.
- [5] Y. Kudo, D. Guardavaccaro, P.G. Santamaria, R. Koyama-Nasu, E. Latres, R. Bronson, L. Yamasaki, M. Pagano, Role of F-box protein β Trcp1 in mammary gland development and tumorigenesis, *Mol. Cell. Biol.* 24 (2004) 8184–8194.
- [6] S. Müreköster, A. Arlt, B. Sipos, M. Witt, M. Großmann, G. Klöppel, U.R. Fölsch, H. Schäfer, Increased expression of the E3-ubiquitin ligase receptor subunit β TRCP1 relates to constitutive nuclear factor- κ B activation and chemoresistance in pancreatic carcinoma cells, *Cancer Res.* 65 (2005) 1316–1324.
- [7] J. Liu, K.G. Kumar, Yu. D. Suresh, S.A. Molton, M. McMahon, M. Herlyn, A. Thomas-Tikhonenko, S.Y. Fuchs, Oncogenic BRAF regulates beta-Trcp expression and NF- κ pA activity in human melanoma cells, *Oncogene* 26 (2007) 1954–1958.
- [8] D. Frescas, M. Pagano, Deregulated proteolysis by the F-box proteins SKP2 and β -TrCP: tipping the scales of cancer, *Nat. Rev. Cancer* 8 (2008) 438–449.
- [9] S. Shafique, S. Younis, H. Niaz, S. Rashid, Elucidation, functional clustering and structural characterization of β TrCP1 substrates through a molecular dynamics study, *Mol. Biosyst.* (2016), <http://dx.doi.org/10.1039/c6mb00189k>.
- [10] J.S. Blees, H.R. Bokesch, D. Rübsamen, K. Schulz, L. Milke, M.M. Bajer, K.R. Gustafson, C.J. Henrich, J.B. McMahon, N.H. Colburn, T. Schmid, Erioflorin stabilizes the tumor suppressor Pcd4 by inhibiting its interaction with the E3-ligase β -TrCP1, *PLoS One* 7 (2012) e46567.
- [11] K. Hirose, H. Wakashin, M. Oki, S.I. Kagami, A. Suto, K. Ikeda, N. Watanabe, I. Iwamoto, Y. Furuchi, H. Nakajima, GS143, an I κ B ubiquitination inhibitor, inhibits allergic airway inflammation in mice, *Biochem. Biophys. Res. Commun.* 26 (374) (2008) 507–511.
- [12] E. Bulatov, A. Ciulli, Targeting Cullin-RING E3 ubiquitin ligases for drug discovery: structure, assembly and small-molecule modulation, *Biochem. J.* 467 (2015) 365–386.
- [13] Z.H. Wu, L.M. Pfeffer, MicroRNA regulation of F-box proteins and its role in cancer, *Semin. Cancer Biol.* 36 (2015) 80–87.
- [14] S.Y. Fuchs, V.S. Spiegelman, K.S. Kumar, The many faces of β -TrCP E3 ubiquitin ligases: reflections in the magic mirror of cancer, *Oncogene* 23 (2004) 2028–2036.
- [15] H.M. Berman, T.N. Bhat, P.E. Bourne, Z. Feng, G. Gilliland, H. Weissig, J. Westbrook, The Protein Data Bank and the challenge of structural genomics, *Nat. Struct. Mol. Biol.* 7 (2000) 957–959.

- [16] S. Kim, P.A. Thiessen, E.E. Bolton, J. Chen, G. Fu, A. Gindulyte, J. Wang, PubChem substance and compound databases, *Nucleic Acids Res.* 44 (D1) (2015) D1202–D1213.
- [17] M.D. Hanwell, D.E. Curtis, D.C. Lonie, T. Vandermeersch, E. Zurek, G. Hutchison, Avogadro: an advanced semantic chemical editor, visualization, and analysis platform, *J. Cheminform* 4 (2012) 17.
- [18] G.M. Morris, R. Huey, W. Lindstrom, M.F. Sanner, R.K. Belew, D.S. Goodsell, A.J. Olson, AutoDock4 and AutoDockTools4: Automated docking with selective receptor flexibility, *J. Comput. Chem.* 30 (2009) 2785–2791.
- [19] L. Guo, Z. Yan, X. Zheng, L. Hu, Y. Yang, J. Wang, A comparison of various optimization algorithms of protein?ligand docking programs by fitness accuracy, *J. Mol. Model.* 20 (2014) 1–10.
- [20] E. Kellenberger, J. odrigo, P. Muller, D. Rognan, Comparative evaluation of eight docking tools for docking and virtual screening accuracy, *Proteins Struct. Funct. Bioinf.* 57 (2004) 225–242.
- [21] G. Jones, P. Willett, R.C. Glen, A.R. Leach, R. Taylor, Development and validation of a genetic algorithm for flexible docking, *J. Mol. Biol.* 267 (1997) 727–748.
- [22] M.D. Eldridge, C.W. Murray, T.R. Auton, G.V. Paolini, R.P. Mee, Empirical scoring functions: I The development of a fast empirical scoring function to estimate the binding affinity of ligands in receptor complexes, *J. Comput. Aided Mol. Des.* 11 (5) (1997) 425–445.
- [23] M.L. Verdonk, J.C. Cole, M.J. Hartshorn, C.W. Murray, R.D. Taylor, Improved protein?ligand docking using GOLD, *Proteins Struct. Funct. Bioinf.* 52 (2003) 609–623.
- [24] A.C. Wallace, R.A. Laskowski, J.M. Thornton, LIGPLOT: a program to generate schematic diagrams of protein-ligand interactions, *Protein Eng.* 8 (1995) 127–134.
- [25] E.C. Meng, E.F. Pettersen, G.S. Couch, C.C. Huang, T.E. Ferrin, Tools for integrated sequence-structure analysis with UCSF Chimera, *BMC Bioinf.* 7 (2006) 339.
- [26] M.J. Abraham, T. Murtola, R. Schulz, S. Páll, J.C. Smith, B. Hess, E. Lindahl, GROMACS: High performance molecular simulations through multi-level parallelism from laptops to supercomputers, *SoftwareX* 1 (2015) 19–25.
- [27] A.W. Schuëttelkopf, D.M. Van Aalten, PRODRG: a tool for high-throughput crystallography of protein?ligand complexes, *Acta Crystallogr. Sect. D Biol. Crystallogr.* 60 (2004) 1355–1363.
- [28] Y. Duan, C. Wu, S. Chowdhury, M.C. Lee, G. Xiong, W. Zhang, R. Yang, P. Cieplak, R. Luo, T. Lee, J. Caldwell, J. Wang, P. Kollman, A point-charge force field for molecular mechanics simulations of proteins based on condensed-phase quantum mechanical calculations, *J. Comput. Chem.* 24 (2003) 1999–2012.
- [29] M.G. Campo, Structural and dynamic properties of SPC/E water, *Pap. Phys.* 2 (2010) 020001.
- [30] M.J. Abraham, J.E. Gready, Optimization of parameters for molecular dynamics simulation using smooth particle-mesh Ewald in GROMACS 4.5, *J. Comput. Chem.* 32 (2011) 2031–2040.
- [31] W. Kabsch, C. Sander, Dictionary of protein secondary structure: pattern recognition of hydrogen-bonded and geometrical features, *Biopolymers* 22 (1983) 2577–2637.
- [32] T. Sindhu, P. Srinivasan, Exploring the binding properties of agonists interacting with human TGR5 using structural modeling, molecular docking and dynamics simulations, *RSC Adv.* 5 (2015) 14202–14213.
- [33] C. Doss, B. Rajith, C. Chakraborty, N. NagaSundaram, S.K. Ali, H. Zhu, Structural signature of the G719S-T790 M double mutation in the EGFR kinase domain and its response to inhibitors, *Sci. Rep.* 4 (2014) 5868.
- [34] I. Sohail, S. Rashid, Molecular dynamics and regulation of butyrylcholinesterase cholinergic activity by RNA binding proteins, *CNS Neurol. Disord. Drug. Targets* 13 (2014) 1366–1377.
- [35] A.K. Mishra, S. Puranik, R.P. Bahadur, M. Prasad, The DNA-binding activity of an AP2 protein is involved in transcriptional regulation of a stress-responsive gene SiWD40, in foxtail millet, *Genomics* 100 (2012) 252–263.
- [36] C. Zhang, F. Zhang, The multifunctions of WD40 proteins in genome integrity and cell cycle progression, *J. Genom.* 3 (2015) 40.
- [37] C. Xu, J. Min, Structure and function of WD40 domain proteins, *Protein Cell* 2 (2011) 202–214.
- [38] Y. Zhao, Y. Sun, Cullin-RING Ligases as attractive anti-cancer targets, *Curr. Pharm. Des.* 19 (2013) 3215–3225.
- [39] G. Wu, G. Xu, B.A. Schulman, P.D. Jeffrey, J.W. Harper, N.P. Pavletich, Structure of a β -TrCP1-Skp1- β -catenin complex: destruction motif binding and lysine specificity of the SCF β -TrCP1 ubiquitin ligase, *Mol. Cell.* 11 (2003) 1445–1456.